

Near-Infrared Imaging Polarimetry Toward Serpens South: Revealing the Importance of the Magnetic Field

K. Sugitani,¹ F. Nakamura,² M. Watanabe,³ M. Tamura,² S. Nishiyama,⁴ T. Nagayama,⁵
R. Kandori,² T. Nagata,⁴ S. Sato,⁵ R. A. Gutermuth,⁶ G. W. Wilson,⁷ and R. Kawabe⁸

ABSTRACT

The Serpens South embedded cluster, which is located at the constricted part in a long filamentary infrared dark cloud, is believed to be in very early stage of cluster formation. We present results of near-infrared (*JHKs*) polarization observations toward the filamentary cloud. Our polarization measurements of near-infrared point sources indicate a well-ordered global magnetic field that is perpendicular to the main filament, implying that the magnetic field is likely to have controlled the formation of the main filament. On the other hand, the sub-filaments, which converge on the central part of the cluster, tend to run along the magnetic field. The global magnetic field appears to be curved in the southern part of the main filament. Such morphology is consistent with the idea that the global magnetic field is distorted by gravitational contraction along the main filament toward the northern part that contains largermass. Applying the Chandrasekhar-Fermi method, the magnetic field strength is roughly estimated to be a few $\times 100 \mu\text{G}$, suggesting that the filamentary cloud is close to magnetically critical as a whole.

Subject headings: polarization — stars: formation — ISM: magnetic fields — ISM: structure — open clusters and associations: individual (Serpens South) — infrared: stars

¹Graduate School of Natural Sciences, Nagoya City University, Mizuho-ku, Nagoya 467-8501, Japan; sugitani@nsc.nagoya-cu.ac.jp.

²National Astronomical Observatory, Mitaka, Tokyo 181-8588, Japan.

³Department of Cosmosciences, Hokkaido University, Kita-ku, Sapporo, Hokkaido 060-0810, Japan.

⁴Department of Astronomy, Kyoto University, Sakyo-ku, Kyoto 606-8502, Japan.

⁵Department of Astrophysics, Nagoya University, Chikusa-ku, Nagoya 464-8602, Japan.

⁶Smith College, University of Massachusetts, Northampton, MA 01063.

⁷Department of Astronomy, University of Massachusetts, Amherst, MA 01003.

⁸Nobeyama Radio Observatory, Nobeyama, Minamimaki, Minamisaku, Nagano 384-1305, Japan.

1. Introduction

It is now widely accepted that stars form predominantly within clusters inside dense clumps of molecular clouds that are turbulent and magnetized. However, how clusters form in such dense clumps remains poorly understood. This is due in part to the lack of the observational characterization of processes involved in cluster formation. In particular, the role of magnetic fields in cluster formation is a matter of debate.

Recent numerical simulations of cluster formation suggest that a moderately-strong magnetic field is needed to impede star formation in molecular clouds in order for the simulated star formation rates to match observed values (Vázquez-Semadeni et al. 2005; Li & Nakamura 2006; Nakamura & Li 2007; Price & Bate 2008). In contrast, Padoan et al. (2001) claim that the magnetic field in molecular clouds should be significantly weak (a few μG) and that the turbulent compression largely controls the structure formation in molecular clouds on scales of a few to several parsecs. Such a very weak magnetic field is necessary to reproduce the core mass spectrum that resembles the stellar initial mass spectrum in shape, in the context of their turbulent fragmentation scenario (Padoan & Nordlund 2002). In this picture, strong magnetic fields sometimes observed in dense clumps and cores are due to local amplification by the turbulent compression. Recent Zeeman measurements in molecular clouds and cores appear to support this idea (Crutcher et al. 2010). If this is the case, the magnetic fields associated with cluster-forming clumps are expected to be distorted significantly by the supersonic turbulent flows.

In order to characterize the magnetic structure of cluster-forming clumps, it is important to uncover the global magnetic field structures associated with as many cluster forming clumps as possible. Polarimetry of background star light is one of the techniques suitable for mapping the magnetic fields in molecular clouds and cores (Tamura et al. 1987) and the technique is now strengthened with wide-field polarimetry by employing large array detectors (e.g., Tamura et al. 2007). As a continuation of our recent polarimetry study of the Serpens cloud core (Sugitani et al. 2010), which revealed an hour-glass shaped magnetic field that implies the global gravitational contraction of the cluster forming clump, we have made near-infrared polarization observations toward Serpens South.

Serpens South is a nearby ($d \sim 260$ pc), embedded cluster, discovered by Gutermuth et al. (2008) in the context of the Spitzer Gould Belt Legacy Survey. The Serpens South cluster appears to be located at the constricted region in a long filamentary cloud or at the joint region of multiple less dense filaments - now referred to as a "hub-filament" structure (Myers 2009). The Serpens cloud core resembles such morphology, although the filamentary structures are much more prominent around Serpens South. In the central part of the cluster, the fraction of protostars (Class 0/I sources) reaches 77 % with a high surface density of

430 pc⁻². This fraction is largest among the cluster-forming regions within the nearest 400 pc. Recently, Bontemps et al. (2010) discovered 5 Class 0 sources in the central core as a part of the Herschel Gould Belt Survey. These observations strongly suggest a very recent initialization of star formation in this region. Therefore, Serpens South is one of the best objects to characterize the initial conditions of cluster formation.

Here, we present the results of our near-infrared polarization measurements, and discuss the role of magnetic fields in the formation of this region.

2. Observations and Data Reduction

Simultaneous polarimetric observations were carried out toward Serpens South in *JHK*s-bands on 2009 August 28 and September 3, and 2010 June 25, August 9, 12, 13, 14, and 15 UT with the imaging polarimeter SIRPOL (polarimetry mode of the SIRIUS camera: Kandori et al. 2006) mounted on the IRSF 1.4 m telescope at the South Africa Astronomical Observatory. The SIRIUS camera is equipped with three 1024 × 1024 HgCdTe (HAWAII) arrays, *JHK*s filters, and dichroic mirrors, which enables simultaneous *JHK*s observations (Nagashima et al. 1999; Nagayama et al. 2003). The field of view at each band is 7'.7 × 7'.7 with a pixel scale of 0".45, and a 3×3 mosaic area centered around (R.A., decl.)_{J2000}=(18^h30^m05^s, -02°03') was covered, including duplicate field observations.

We obtained 10 dithered exposures, each 10 or 15 s long, at four wave-plate angles (0°, 22°.5, 45°, and 67°.5 in the instrumental coordinate system) as one set of observations and repeated this nine or six times, respectively. Thus, the total on-target exposure time for each field was 900 s per wave-plate angle. Sky images were also obtained in between target observations. Self sky images were also used with the sky images to make better median sky images. The average seeing was ∼1."4 at *K*s during the observations with a range of ∼1."2–1."6. Twilight flat-field images were obtained at the beginning and/or end of the observations. Standard reduction procedures were applied with IRAF. Aperture polarimetry was performed at *H* and *K*s with an aperture of ∼FWHM by using APHOT of the DAOPHOT package. No polarimetry for *J* band sources was done due to their much smaller number, compared with those of *H* and *K*s band sources. The 2MASS catalog (Skrutskie et al. 2006) was used for absolute photometric calibration. See Sugitani et al. (2010) for more details of the data reduction procedure and the method to derive the polarization degree (*P*) and its error (ΔP), and the polarization angle (θ in P.A.) and its error ($\Delta\theta$).

3. RESULTS and DISCUSSION

3.1. Magnetic Field Structure toward Serpens South

We have measured H and K_s polarization for point sources, in order to examine the magnetic field structure. Only the sources with photometric errors of <0.1 mag and $P/\Delta P > 3.0$ were used for analysis.

Figures 1a and 2a present the polarization degree versus the $H - K_s$ color for sources having polarization errors of $< 0.3\%$ at H and K_s , respectively. There is a tendency for the upper envelope of the plotted points to increase with $H - K_s$, and the average polarization degree is slightly smaller at K_s than at H for the same $H - K_s$ color. These are consistent with the origin of the polarization being dichroic absorption. Therefore, here we assume the polarization vectors as the directions of the local magnetic field average over the line of sight of the sources. These sources, except those of low $H - K_s$ colors, appear to have the maximum polarization efficiencies of $P_H/([H - K_s] - 0.2) = 6.6$ and $P_{K_s}/([H - K_s] - 0.2) = 4.4$, where we adopt $H - K_s = 0.2$ as an offset of the intrinsic $H - K_s$ color, because the 2MASS point sources with good photometric qualities are mostly located on the reddening belt that begins from the position of $(J - H, H - K_s) = (\sim 0.7, \sim 0.2)$ on the $J - H$ versus $H - K_s$ diagram, within a $1^\circ \times 1^\circ$ area centered at Serpens South.

Figures 3 and 4 present H and K_s -band polarization vectors of $P/\Delta P > 3.0$, excluding sources with polarizations larger than the above maximum polarization, superposed on 3×3 mosaic H and K_s -band images, respectively. In general, the global magnetic field structures deduced from the H and K_s -band data seem to be the same. Most of the vectors are roughly aligned with the NE-SW direction with the exception of those appearing in the NE and SW corners of the map. Two distribution peaks are clearly seen in the histogram of the K_s -band vector angles, although a sub-peak at H can be barely seen (Figure 5). Our two-Gaussian fit analysis for the K_s -band vectors indicates that the mean angle of the main peak is $52.9^\circ \pm 3.0^\circ$ with a standard deviation of $22.8^\circ \pm 2.8^\circ$ and that the mean angle of the sub-peak is $0.0^\circ \pm 5.2^\circ$ with a standard deviation of $16.6^\circ \pm 4.3^\circ$. The low number density of background stars toward the NE corner area suggests a molecular cloud or filament, other than the Serpens South cloud, having a different magnetic field structure. On the other hand, toward the SW corner area, no clear signs of clouds are seen with high density of background stars. To investigate this further we examined the sources within a zone enclosed by the dotted lines toward the SW corner of the maps. Unlike in the main filament, there is no tendency that the degree of polarization in this zone increases as an increase of $H - K_s$ color, and the degrees of polarization are relatively low with values $\lesssim 3\%$ at H and $\lesssim 2\%$ at K_s (except a few sources) in Figures 1b and 2b. Thus, the polarization in this SW area

may not be dominated by the dichroic absorption of the Serpens South cloud and is likely contaminated by either foreground or background interstellar polarization, although it could be also possible that the line-of-sight component of the magnetic field is dominant toward the SW corner area.

We apply a cut on the degree of polarization of at least 3% in P_H and 2% in P_{K_s} in order to insure that we are sampling the magnetic field associated with the dichroic absorption of the material in Serpens South. Figures 6 and 7 present the polarization vectors for the sources of $P_H > 3.0\%$ and $P_{K_s} > 2.0\%$, respectively, superposed on 1.1mm dust continuum image (Gutermuth et al. 2011), which was taken with the 144 pixel bolometer camera AzTEC (Wilson et al. 2008) mounted on the Atacama Submillimeter Telescope Experiment (ASTE). Figure 8 presents the schematic drawing of the filaments and the magnetic field directions toward the Serpens South region. The illustrations of the filaments were deduced from this continuum image. The directions of the magnetic field were deduced from the the H -band polarization vectors in Figure 6.

The 1.1 mm dust continuum image clearly shows a main filament that is elongated toward the NW and SE directions from the central part of Serpens South. Along this main filament, the magnetic field is roughly perpendicular to it, although some small deviation is seen. This ordered magnetic configuration suggests that the magnetic field is strong enough to regulate the whole structure of the main filament and, therefore, that the formation of the main filament has proceeded under the influence of the magnetic field.

Also the 1.1 mm dust continuum image shows sub-filaments that converge on the central part of the cluster or intersect the main filament (Figures 6, 7 and 8). These sub-filaments are also seen in the column density map of Aquila (André et al. 2010). In contrast to the main filament, the magnetic field appears to be nearly parallel to the elongation directions of the sub-filaments, except in some parts of the sub-filaments. The southern sub-filament has a more complicated structure than a simple elongated structure and its global elongation seems parallel to the magnetic field, although some parts seem perpendicular or diagonal to the magnetic field. The east-southeast sub-filament is a long filament that stretches from the central part of the cluster toward the east-southeast direction, and appears to have some parts parallel to the magnetic field and some other parts diagonal to the magnetic field. Near the convergent point on the main filament, this ESE sub-filament appears to change its elongation direction from the ESE-WNW direction to the E-W direction and to split into a few, thinner filaments that are connected to the main filament (see Figure 9, and also Fig. 1 of Gutermuth et al. 2008). Toward this convergent point, the magnetic field also seems to be nearly perpendicular to the main filament just like the other sub-filaments. These suggest that all the sub-filaments intersect the main filament along the magnetic field, i.e.

these sub-filaments could be outflows from the cluster or inflows toward the main filament. Recent CO (3-2) observations toward Serpens South suggest that CO (3-2) outflow lobes are anti-correlated with the sub-filaments (Nakamura et al. 2011), preferring the inflow view of the sub-filaments. In case of the inflows, these sub-filaments could be important as mass supply agents of the cluster.

Looking at the overall magnetic field structure in the entire observed region, we can recognize that the magnetic field is curved toward the cluster, particularly in the southern area of the observed region (Figures 6, 7 and 8). Although the origin of this large-scale curved magnetic field remains unclear, such morphology is consistent with the idea that the global magnetic field is distorted by gravitational contraction along the main filament toward the northern part of the main filament, which probably contains the majority of the mass in the Serpens South cloud. However, we should wait for the detailed analysis of the dust continuum data (e.g., Gutermuth et al. 2011) and/or molecular line data in order to know whether the northern part have enough mass to cause the large-scale curved magnetic field observed here.

3.2. Rough Estimate of the Magnetic Field Strength

We roughly estimate the magnetic field strength toward two (north, and south) zones enclosed by dotted lines in Figure 8, where in the H -band polarization map (Figure 6) the local number density of the polarization vectors is relatively large and the polarization vectors seem to be locally well-ordered, using the Chandrasekhar-Fermi (CF) method (Chandrasekhar & Fermi 1953). Here, we calculate the plan-of-the-sky component of the magnetic field strength, B_{\parallel} , using the equation of the CF method (e.g., eq. 4 of Houde 2004) and a correction factor, C , for the CF method (Houde 2004; Houde et al. 2009), where we adopt $C \sim 0.3$ following Sugitani et al. (2010). In this calculation, we use the H -band sources in Figure 6, due to the sample number larger than that of the K s-band sources in Figure 7.

For 21 sources toward the north zone, an average θ in P.A. is calculated to be $51.1^{\circ} \pm 9.6^{\circ}$, and an average $H - K$ s color to be 1.09 ± 0.15 mag. Removing the dispersion due to the measurement uncertainty of the polarization angle of 4.7° , the intrinsic dispersion of the polarization angle (σ_{θ}) of 8.4° is obtained. From the average $H - K$ s color, we estimate A_V by adopting the color excess equation of $H - K$ color, $E(H - K) = [H - K]_{\text{observed}} - [H - K]_{\text{intrinsic}}$ (e.g., Lada et al. 1994), and the reddening law, $E(H - K) = 0.065 \times A_V$ (Cohen et al. 1981). With the standard gas-to-extinction, $N_{\text{H}_2}/A_V \sim 1.25 \times 10^{21} \text{ cm}^{-2} \text{ mag}^{-1}$ (Dickman 1978), H_2 column density can be roughly obtained as $N \sim 1.9 \times 10^{22} \times E(H - K) \text{ cm}^{-2}$. Adopting

a distance from the filament axis of $\sim 2'$ ($l/2 \sim 0.15$ pc at $d \sim 260$ pc) as a half of the depth of this area, and $H - K = 0.2$ as the intrinsic $H - K$ color, we can approximately derive a column density of $\sim 1.7 \times 10^{22}$ cm $^{-2}$ and a number density ($n \sim N/l$) of $\sim 1.5 \times 10^4$ cm $^{-3}$. On the basis of HCO $^+$ (4-3) observations, we estimate the typical FWHM velocity width of ~ 1.5 – 2 km s $^{-1}$ near the cluster (Nakamura et al. 2011). Adopting this value to derive the velocity dispersion (σ_v), a mean molecular mass ($\mu=2.3$), and the mass of a hydrogen atom (m_{H}), we obtain $B_{\parallel} \sim 150$ μG . For 25 sources toward the south zone, with $\bar{\theta} = 33.8^\circ \pm 6.9^\circ$, $[H - K_s] = 1.05 \pm 0.18$ mag., the θ measurement uncertainty of 5.2° , and $l \sim 0.45$ pc, $B_{\parallel} \sim 200$ μG is obtained. Here we adopted $d = 260$ pc, following Gutermuth et al. (2008) and Bontemps et al. (2010). However, they also mentioned the possibility of a larger distance up to 700 pc. In case of the larger distance, B becomes smaller by a factor of $(d/260\text{pc})^{-0.5}$ in these estimates.

The dynamical state of a magnetized cloud core is measured by the ratio between the cloud mass and the magnetic flux, i.e., the mass-to-flux ratio, which is given by $M_{\text{cloud}}/\Psi = \mu m_{\text{H}} N/B \sim 0.5$ – $0.7 \times (M_{\text{cloud}}/\Psi)_{\text{critical}}$ for these two zones, where $(M_{\text{cloud}}/\Psi)_{\text{critical}}$ is the critical value for a magnetic stability of the cloud ($= (4\pi^2 G)^{-1/2}$; Nakano & Nakamura 1978). Here, we assumed that the magnetic field is almost perpendicular to the line-of-sight. The estimated mass-to-flux ratios are close to the critical, implying that the magnetic field is likely to play an important role in the cloud dynamics and, thus, star formation significantly.

3.3. Conclusions

We have presented near-infrared imaging polarimetry toward the Serpens South cloud. The main findings are summarized as follows.

1. The H and K s-band polarization measurements of near-infrared point sources indicated a well-ordered global magnetic field that is nearly perpendicular to the main filament with a mean position angle of $\sim 50^\circ$. This implies that the magnetic field is likely to have controlled the formation of the main filament. On the other hand, the sub-filaments, which converge on the central part of the cluster, tend to run along the magnetic field, indicating a possibility that they are inflows or outflows along the magnetic field.

2. The global magnetic field appears to be curved in the southern part of the observed region. This curved morphology suggests an idea that the global magnetic field is distorted by gravitational contraction along the main filament toward the northern part where the mass of the Serpens South cloud seems to be mostly concentrated.

3. Applying the Chandrasekhar-Fermi method, the magnetic field strength is roughly

estimated to be a few $\times 100 \mu\text{G}$ in two zones along the main filament. The mass-to-flux ratios in these zones indicate that the filamentary cloud is close to magnetically critical as a whole.

4. All the above results show that the magnetic field appears to significantly influence the dynamics of the Serpens South cloud, which is associated with the cluster that is considered to be in the very early stage of cluster formation. This does not appear to support the weak magnetic field models of molecular cloud evolution/cluster formation (e.g., Padoan et al. 2001), at least not for the Serpens South cloud.

We are grateful for the support of the staff members of SAAO during the observation runs. K. S. thanks Y. Nakajima for assisting in the data reduction with the SIRPOL pipeline package. This work was partly supported by Grant-in-Aid for Scientific Research (19204018, 20403003) from the Ministry of Education, Culture, Sports, Science and Technology of Japan.

REFERENCES

- André, P., et al. 2010, *A&A*, 518, L102
- Bontemps, S., et al. 2010, *A&A*, 518, L85
- Chandrasekhar, S., & Fermi, E. 1953, *ApJ*, 118, 113
- Cohen, J. G., Frogel, J. A., Persson, S. E., & Elias, J. H. 1981, *ApJ*, 249, 481
- Crutcher, R. M., Wandelt, B., Heiles, C., Falgarone, E. Troland, T. H. 2010, *ApJ*, 725, 466
- Dickman, R. L. 1978, *ApJS*, 37, 407
- Gutermuth, R. A., et al. 2011, in preparation
- Gutermuth, R. A., et al. *ApJ*, 2008, 673, L151
- Houde, M. 2004, *ApJ*, 616, L111
- Houde, M., Vaillancourt, J. E., Hildebrand, R. H., Chitsazzadeh, S., & Kirby, L. 2009, *ApJ*, 706, 1504
- Kandori, R., et al. 2006, *Proc. SPIE*, 6269, 626951
- Lada, C., Lada, E., Clemens, & Bally, J., 1994, *ApJ*, 429, 694

- Li, Z.-Y., & Nakamura, F., 2006, *ApJ*, 640, L187
- Myers, P. C. 2009, *ApJ*, 700, 1609
- Nagashima, C., et al. 1999, in *Star Formation 1999*, ed. T. Nakamoto (Nobeyama: Nobeyama Radio Observatory), 397
- Nagayama, T., et al. 2003, *Proc. SPIE*, 4841, 459
- Nakamura, F., & Li, Z.-Y., 2007, *ApJ*, 662, 395
- Nakamura, F., et al. 2011, in preparation
- Nakano, T., & Nakamura, T. 1978, *PASJ*, 30, 671
- Padoan, P., Juvela, M., Goodman, A. A., & Nordlund, A. 2001, *ApJ*, 553, 227
- Padoan, P., & Nordlund, A. 2002, *ApJ*, 576, 870
- Price, D. J., & Bate, M. R., 2008, *MNRAS*, 385, 1820
- Ridge, N. A., Wilson, T. L., Megeath, S. T., Allen, L. E., & Myers, P. C. 2003, *AJ*, 126, 286
- Skrutskie, M. F., et al. 2006, *AJ*, 131, 1163
- Sugitani, K., et al. 2010, *ApJ*, 716, 299
- Tamura, M., Nagata, T., Sato, S., & Tanaka, M. 1987, *MNRAS*, 224, 413
- Tamura, M., et al. 2007, *PASJ*, 59, 467
- Vázquez-Semadeni, E., Kim, J., & Ballesteros-Paredes, J., 2005, *ApJ*, 630, L49
- Wilson, G. W., et al., 2008, *MNRAS*, 386, 807

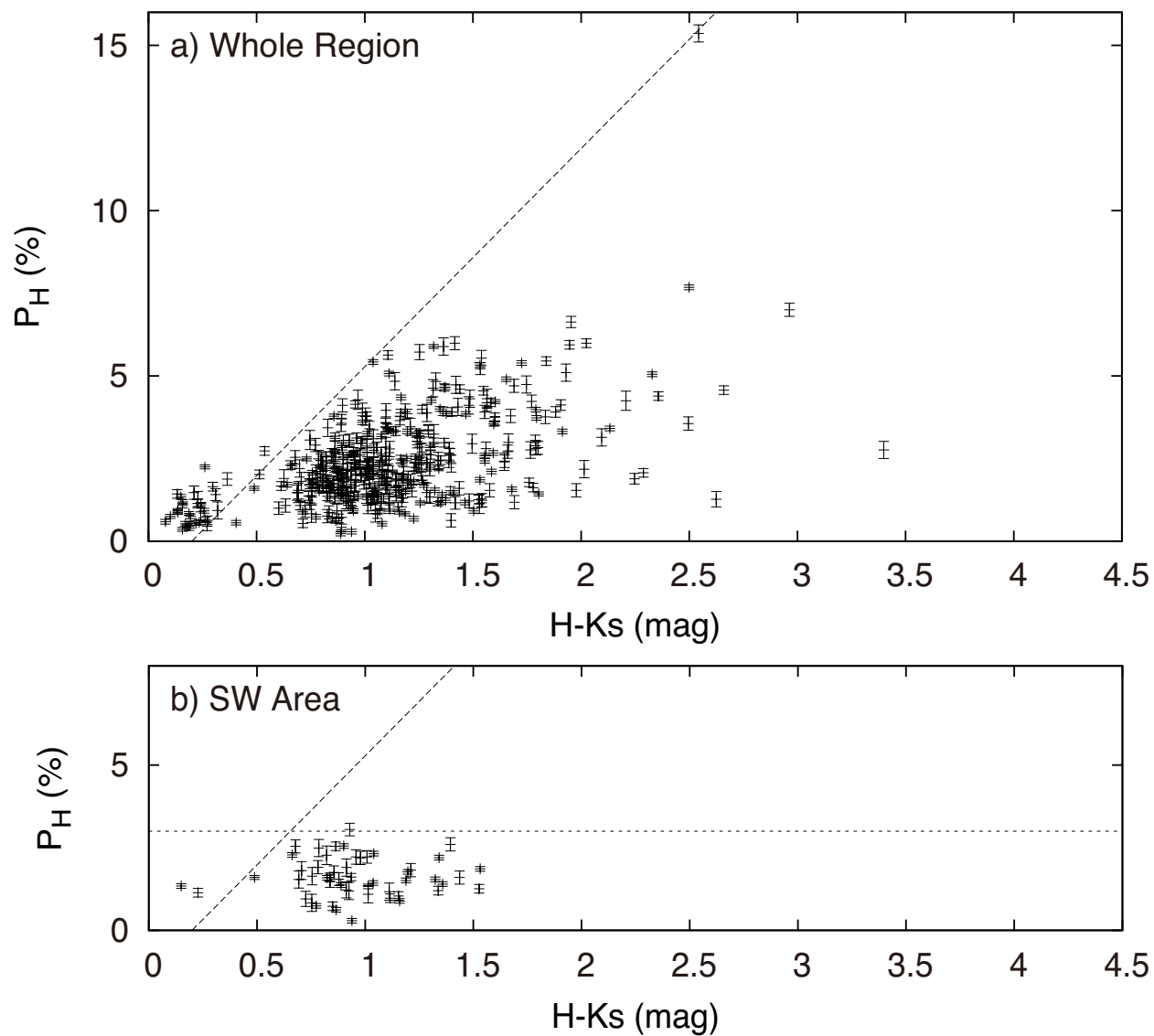


Fig. 1.— Polarization degree at H versus $H - K_s$ color diagram for sources having polarization errors of $< 0.3\%$ in (a) the whole region and (b) the SW area. YSOs/YSO candidates identified by Gutermuth et al. (2008) and Bontemps et al. (2010) are not included. The lines of the adopted maximum polarization efficiency of $P_H = 6.6([H - K_s] - 0.2)$ are shown both in the top and bottom panels, and the line of $P_H = 3.0$ is shown in the bottom panel.

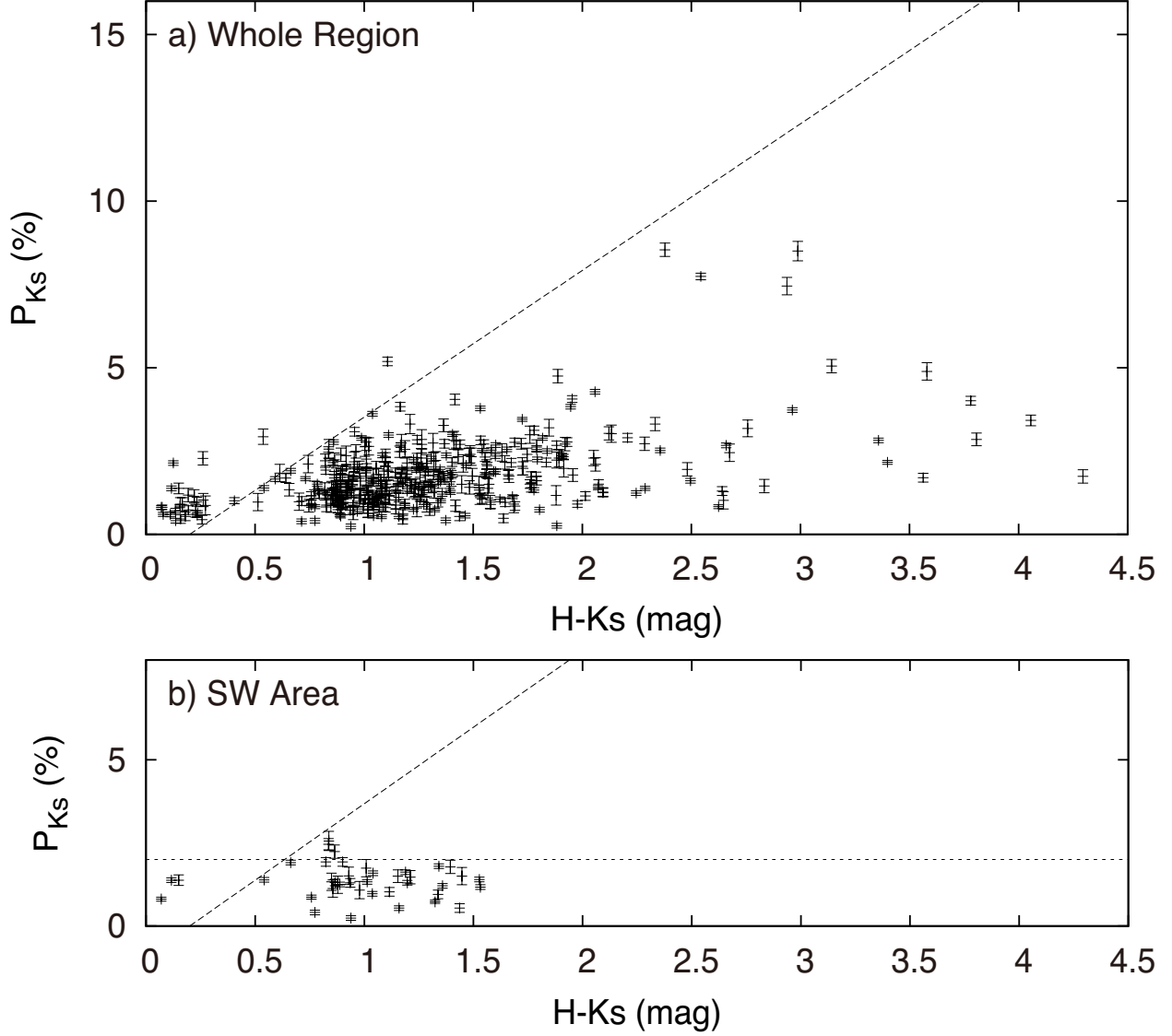


Fig. 2.— Polarization degree at K_s versus $H - K_s$ color diagram for sources having polarization errors of $< 0.3\%$ in (a) the whole region and (b) the SW area. YSOs/YSO candidates identified by Gutermuth et al. (2008) and Bontemps et al. (2010) are not included. The lines of the adopted maximum polarization efficiency of $P_{K_s} = 4.4([H - K_s] - 0.2)$ are shown both in the top and bottom panels, and the line of $P_{K_s} = 2.0$ is shown in the bottom panel.

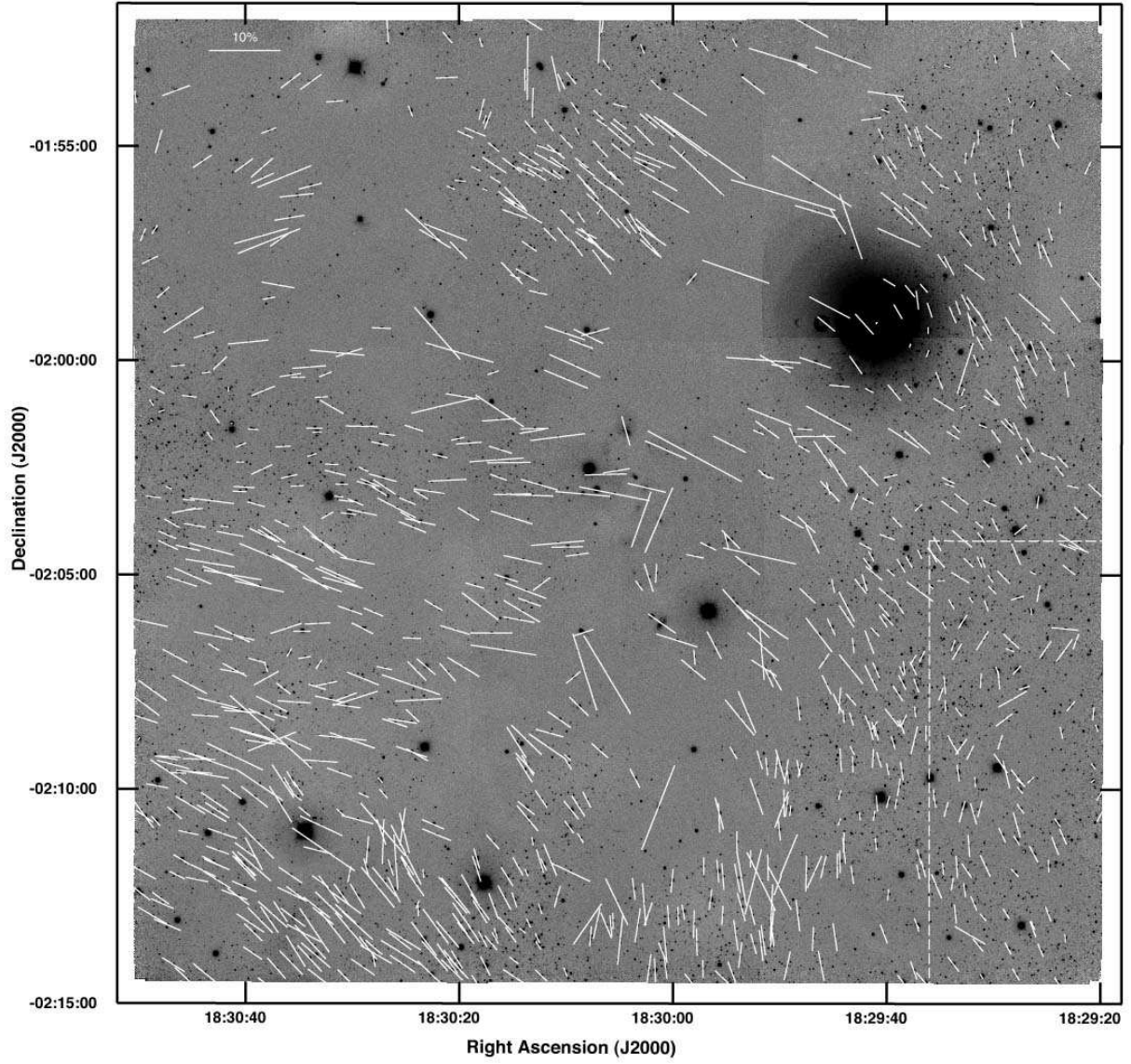


Fig. 3.— H -band polarization vector map toward Serpens South for point sources having $P/\Delta P > 3.0$ and $P < 6.6([H - K_s] - 0.2)$, superposed on the H -band image. The Serpens South cluster is located toward the center of the image.

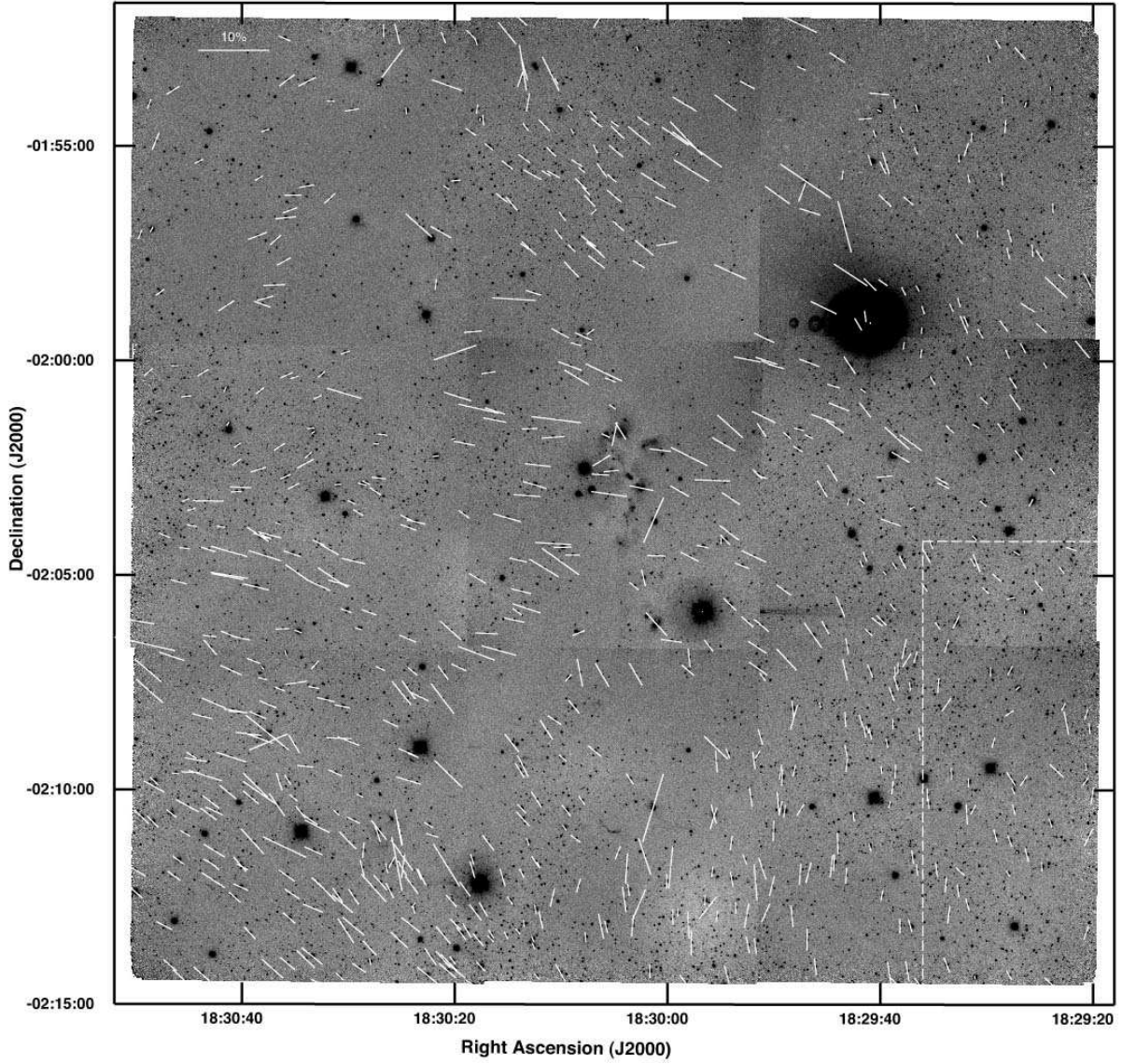


Fig. 4.— K_s -band polarization vector map toward Serpens South for point sources having $P/\Delta P > 3.0$ and $P < 4.4([H - K_s] - 0.2)$, superposed on the K_s -band image. The Serpens South cluster is located toward the center of the image.

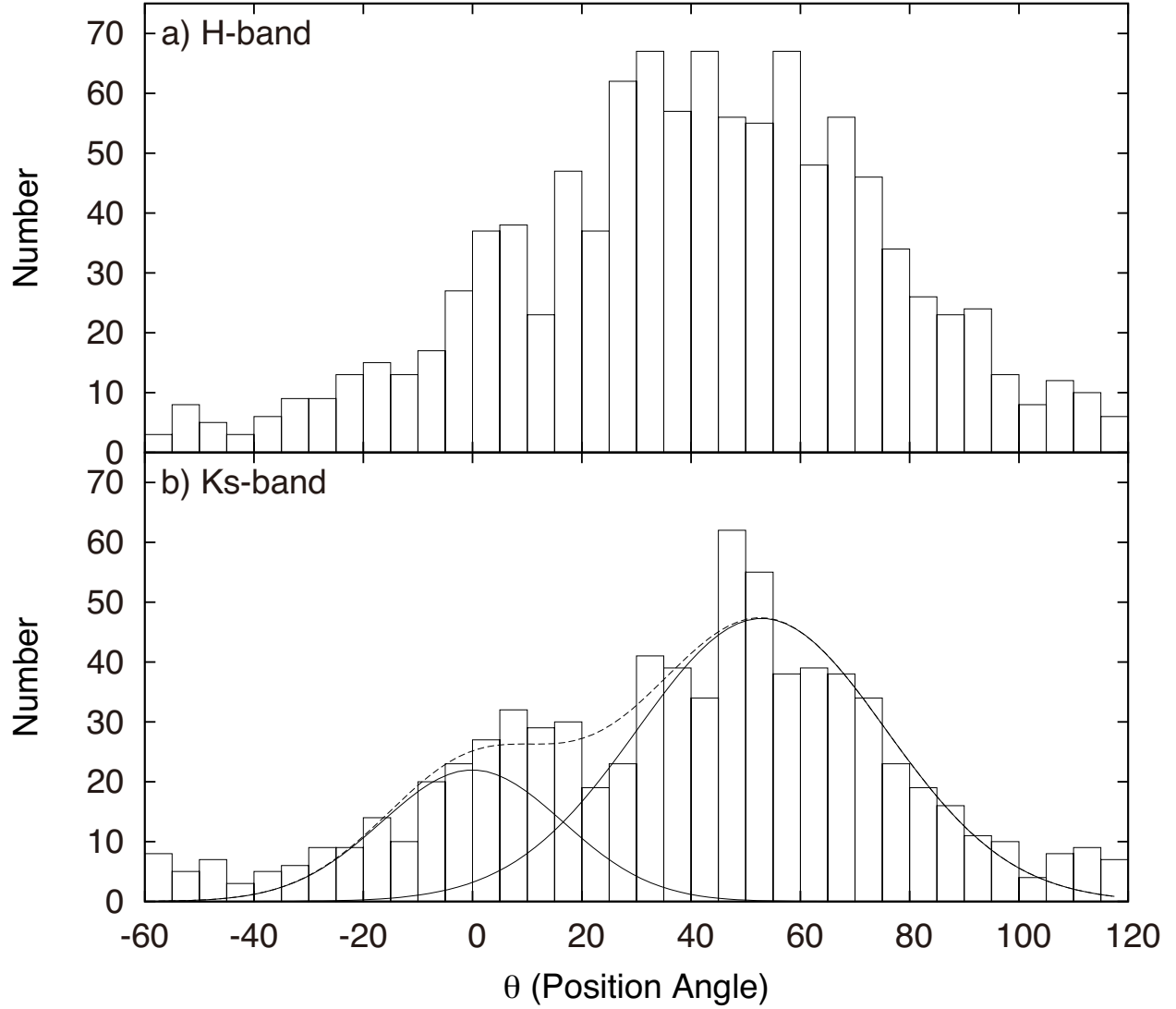


Fig. 5.— Histograms of the position angles of a) H -band vectors for point sources of $P/\Delta P > 3.0$ and $P < 6.6([H - K_s] - 0.2)$, and b) K_s -band vectors for point sources of $P/\Delta P > 3.0$ and $P < 4.4([H - K_s] - 0.2)$. A two-Gaussian fit is shown on the K_s -band histogram.

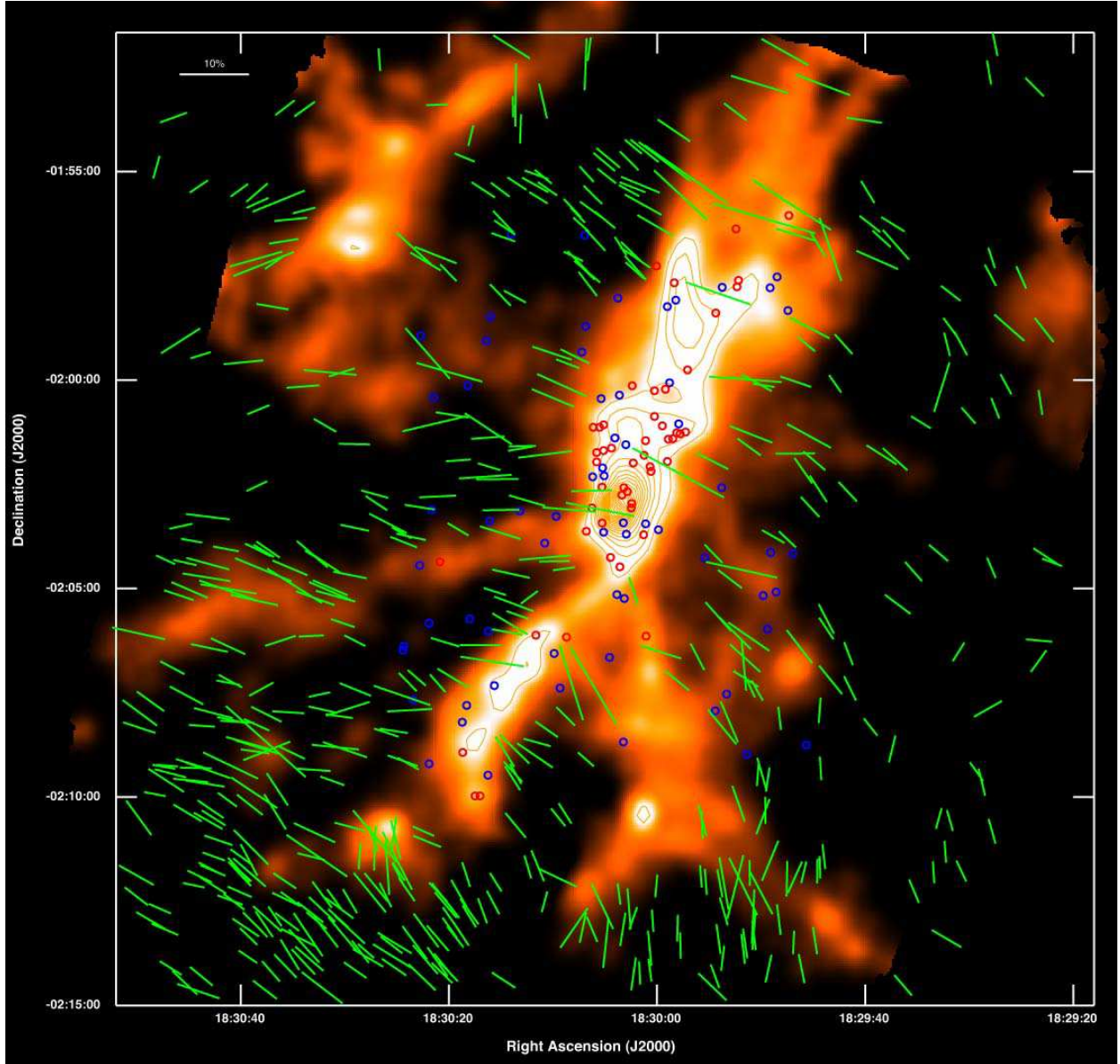


Fig. 6.— *H*-band polarization vector map toward Serpens South for point sources having $P/\Delta P > 3.0$, $P < 6.6([H - K_s] - 0.2)$, and $P > 3.0\%$, superposed on 1.1mm dust continuum image of ASTE/AzTEC (Gutermuth et al. 2011). YSOs identified by Gutermuth et al. (2008) and Bontemps et al. (2010) are not included, but those of Gutermuth et al. (2008) are indicated by red (class 0/I) and blue (class II) open circles.

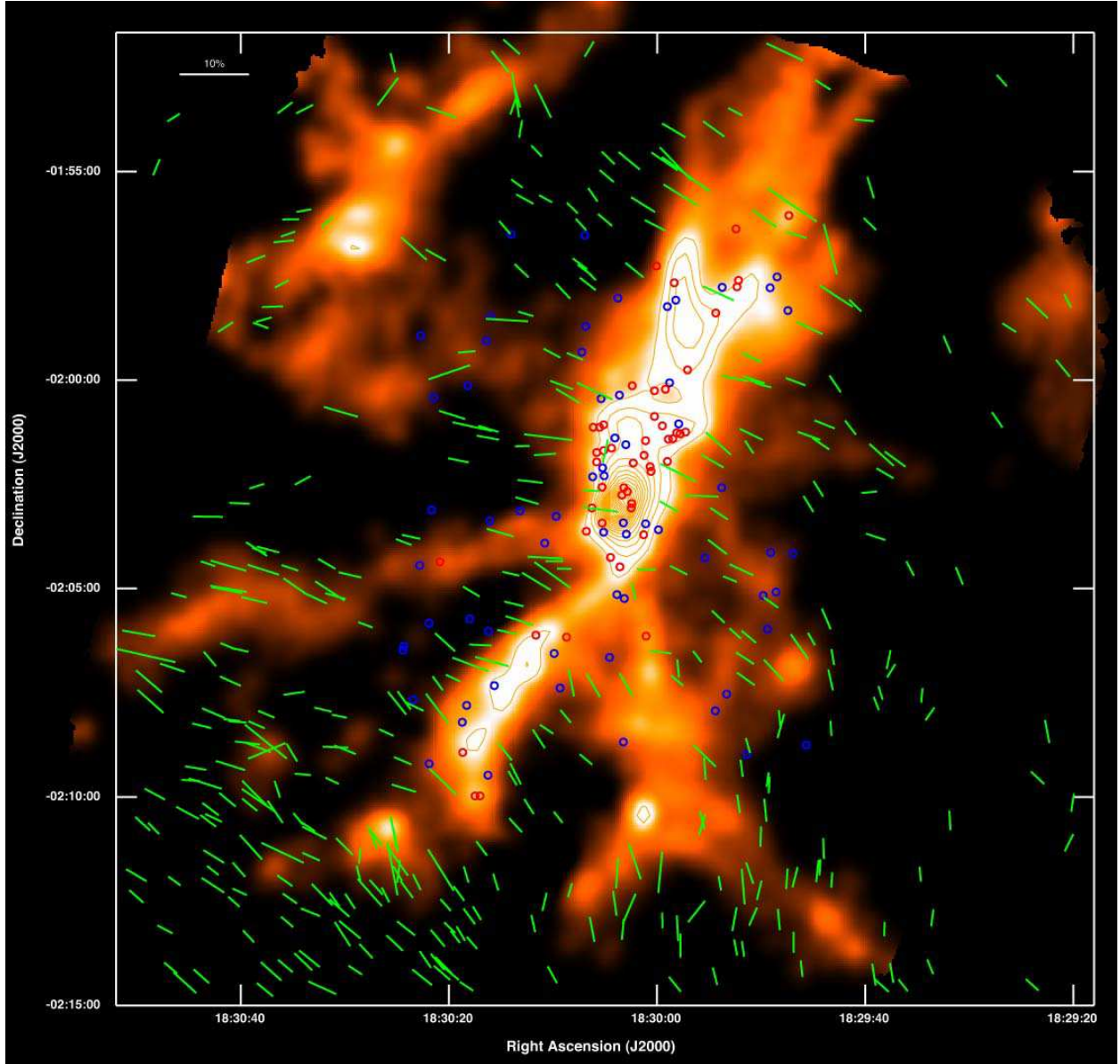


Fig. 7.— K_s -band polarization vector map toward Serpens South for point sources having $P/\Delta P > 3.0$, $P < 4.4([H - K_s] - 0.2)$, and $P > 2.0\%$, superposed on 1.1mm dust continuum image of ASTE/AzTEC (Gutermuth et al. 2011). YSOs identified by Gutermuth et al. (2008) and Bontemps et al. (2010) are not included, but those of Gutermuth et al. (2008) are indicated by red (class 0/I) and blue (class II) open circles.

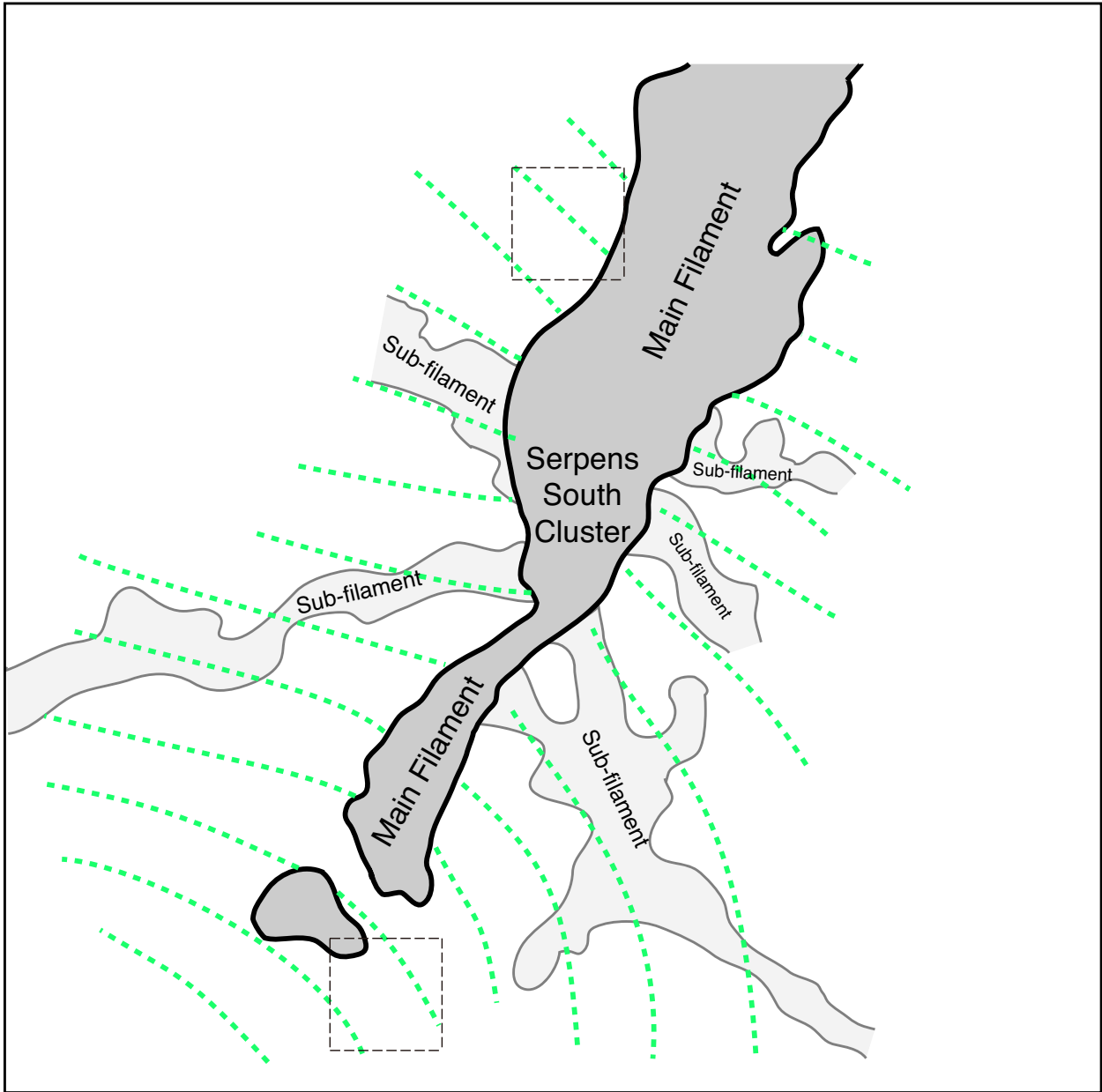


Fig. 8.— Schematic drawing of the main and sub-filaments of the Serpens South cloud. The outlines of the filaments and the magnetic field lines are shown by black lines and green dotted lines, respectively. The outlines of the filaments were drawn based on the 1.1mm dust continuum image (Gutermuth et al. 2011) and the magnetic field lines were deduced from the H -band polarization vectors of Figure 6. In this figure, the magnetic field lines presents only the direction of the magnetic field, not the strength of the magnetic field. The boxes outlines by black, dotted lines indicate the zones where the strength of the magnetic field is roughly estimated.

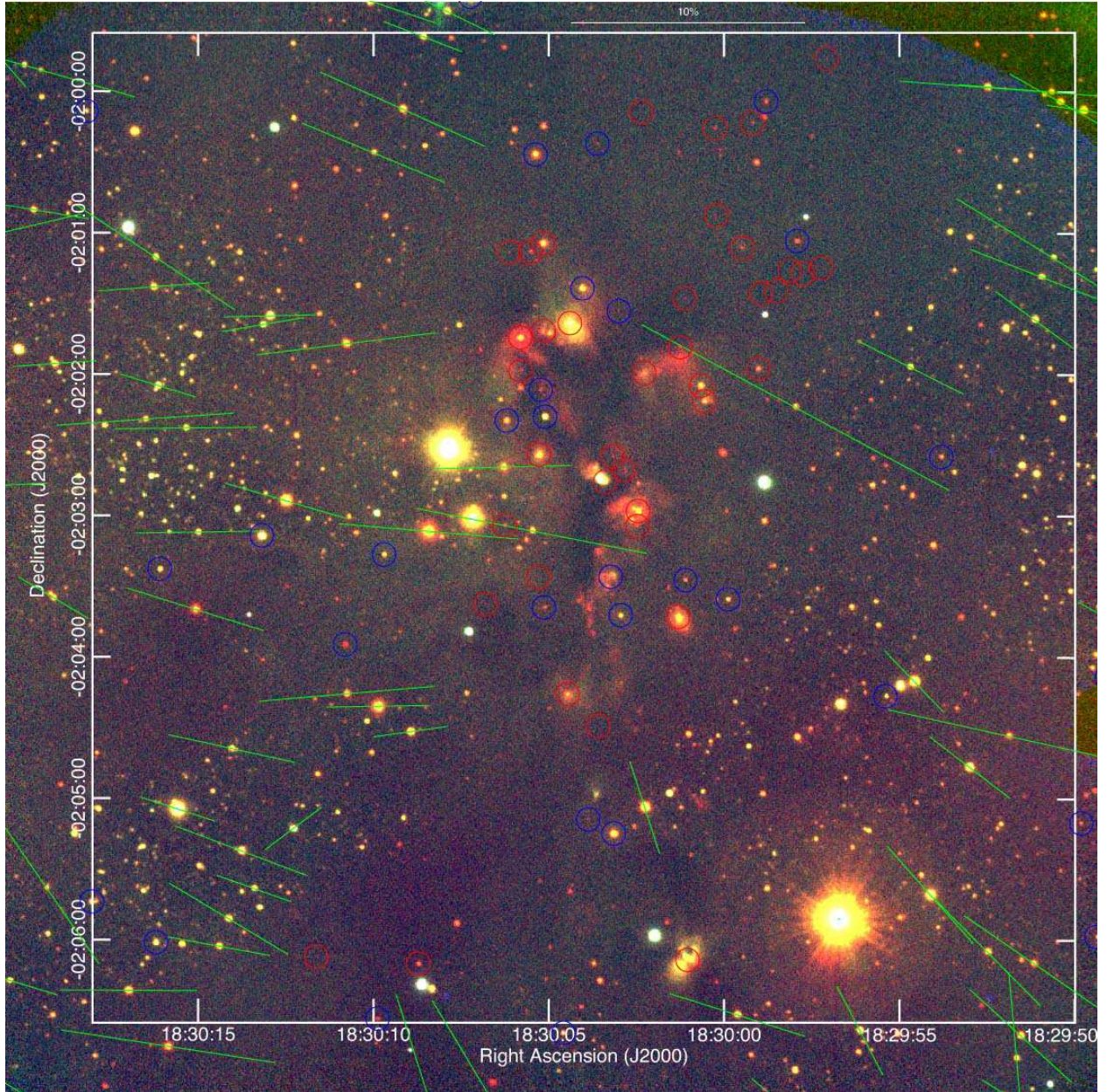


Fig. 9.— H -band polarization vector map, superposed on a closeup, JHK_s composite color image of Serpens South (R: K_s , G: H , B: J). Only the vectors of the sources of $P/\Delta P > 3.0$, $P < 6.6([H - K_s] - 0.2)$ and $P > 3.0\%$, are shown. YSOs identified by Gutermuth et al. (2008) are indicated by red (Class 0/I) and blue (Class II) open circles, but their polarization vectors are not shown.